

---

# Impeding Hohlraum Plasma Stagnation in Inertial Confinement Fusion

The symmetry requirements for achieving ignition are fundamental and impose strict constraints on inertial confinement fusion (ICF).<sup>1–7</sup> The tolerable drive asymmetry of an implosion, in a time-integrated sense, is less than 1% to 2% and depends on the ignition margin.<sup>3,4</sup> In the indirect-drive approach to ICF, low-mode-number implosion asymmetries are a major concern because the quasi-uniform hohlraum radiation field provides drive with minimal high-mode-number nonuniformities.<sup>3–8</sup> An example of such an asymmetry would be a time-integrated P2 (second-order Legendre polynomial) nonuniformity that could lead to different radial velocities and densities at pole and equator, converting less kinetic energy into internal energy and resulting in a higher drive energy required for ignition.

The high-Z plasma from the wall blowoff, usually gold (Au) or uranium (U), which causes motion in the laser-absorption region and alters the spatial distributions of x-ray energy sources and sinks, has been shown to cause low-mode-number implosion asymmetries.<sup>3–8</sup> The blowoff quickly fills the interior of an initially empty (optically thin) hohlraum, leading to early on-axis plasma stagnation.<sup>3–8</sup> The stagnated plasma has high pressure and can asymmetrically compress the capsule.

To achieve the required drive symmetry, the motion of the laser-deposition (x-ray emission) region must be minimized. Two proposed approaches are to overcoat a hohlraum wall surface with a low-Z liner and to fill a hohlraum interior with low-Z gas.<sup>4</sup> Neither the liner nor the fill gas stops the wall blowoff; however, they displace the low-density plasmas. In the first approach, plasma jets form because of the interaction of pairs of adjacent, expanding plumes of low-Z liner blowoff.<sup>4,9</sup> The radially moving jets are supersonic and quickly stagnate at the hohlraum interior, resulting in asymmetries in both the drive and the capsule implosion. The ignition campaign at the National Ignition Facility (NIF) currently adopts the second approach.<sup>3–7</sup> Hohlräume are filled with helium-4 gas<sup>6</sup> at a pressure  $\sim 0.4$  atm (when fully ionized,  $n_e \sim 0.04 n_{\text{crit}}$ , the critical electron density for 0.35- $\mu\text{m}$  laser light). The gas is

contained with thin polyimide windows over the laser entrance holes (LEH's).

This article presents the first proton radiography observations of the effects of gas fill on impeding the hohlraum plasma stagnation. The experiments, illustrated schematically in Fig. 125.7(a), were performed at the Omega Laser Facility.<sup>10</sup> Radiographic images were made with 15-MeV protons at various implosion times through the LEH.<sup>9,11</sup> Figure 125.7 shows two different types of images: proton fluence versus position [Fig. 125.7(b)] and proton mean energy versus position [Fig. 125.7(c)]. The proton fluence piles up in the gaps between the two expanding plasma plumes and in the region between the imploding capsule and the expanding plasmas, forming a five-prong, asterisk-like pattern—a consequence of OMEGA's laser-beam distribution.<sup>9,11</sup> Contrary to earlier experiments that showed a deficit in proton fluence in these regions for vacuum hohlräume,<sup>9,11</sup> this fluence surplus suggests that no high-density plasma jets were formed. The fill gas along the laser beam's path is fully ionized. The interfaces between the gas plasma and the Au wall blowoff are constrained near the wall's surface [Fig. 125.7(b), indicated by the open arrows]. Figure 125.8 shows the measured Au-wall plasma-fill gas interface radius as a function of time compared with the sound speed  $\left[ C_s \propto (Z T_e m_i^{-1})^{1/2} \right]$  that sets the scale for hydrodynamic rarefaction expansion in vacuum.<sup>11,12</sup> The expansion speed of the Au blowoff is estimated to be  $\sim (2.1 \pm 0.3) \times 10^7 \text{ cm s}^{-1}$ , which is slower than  $C_s \sim 2.5 \times 10^7 \text{ cm s}^{-1}$ , indicating that the wall blowoff's expansion has been compressed by the fill gas.<sup>13</sup> These measurements show that the fill gas impedes the wall plasma expansion.

An additional interface appears in the region around the imploding capsule [1.65 ns, Fig. 125.7(b)]. It is identified as the interface between the capsule's CH ablation and the fill-gas plasma. Because the implosion is nearing the deceleration phase, with the typical implosion velocity,  $v_{\text{imp}} \left[ \propto I_{15}^{1/8} \ln(m_0/m) \right] \sim 2$  to  $3 \times 10^7 \text{ cm s}^{-1}$  and velocity of outward-moving ablated cap-

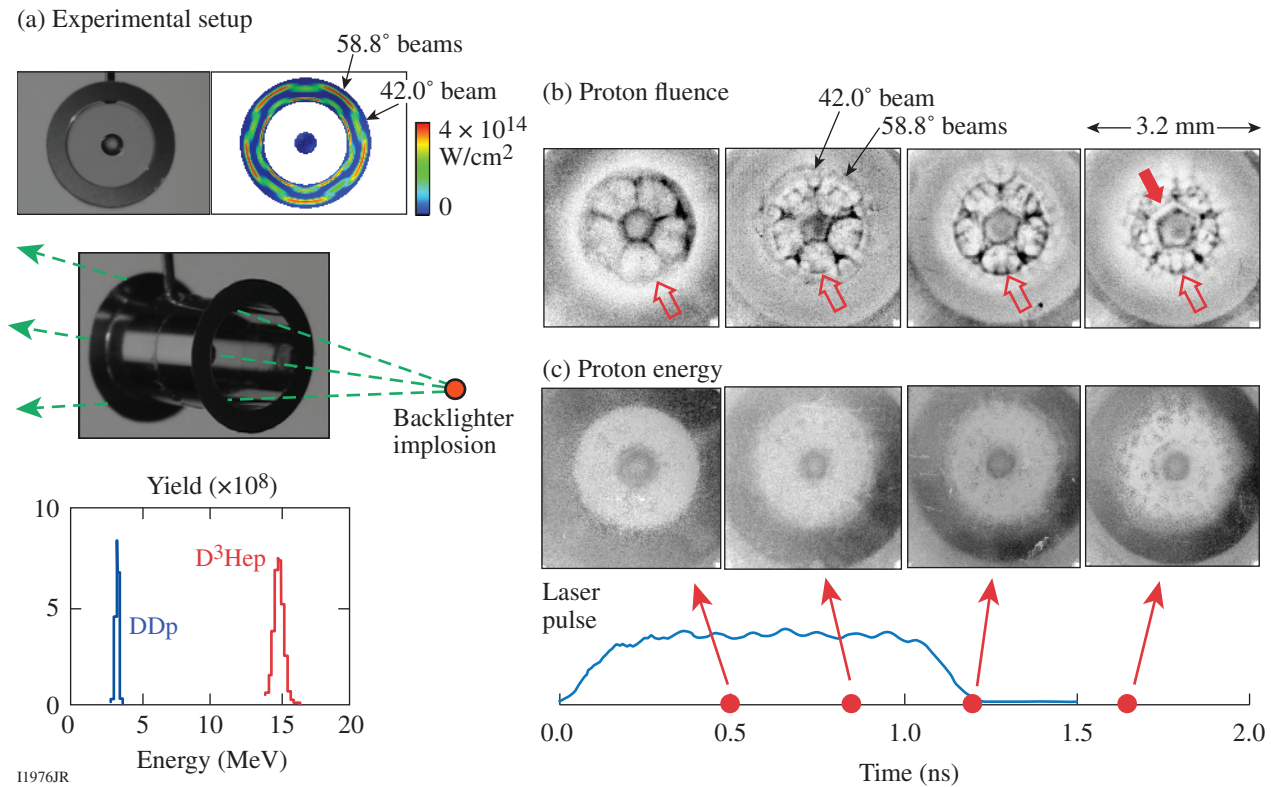


Figure 125.7

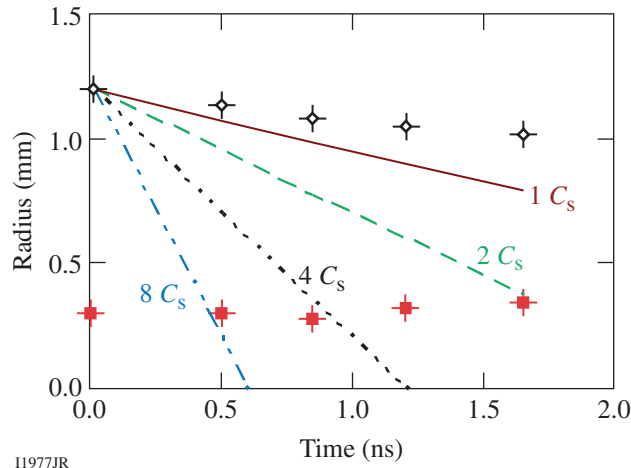
(a) Experimental setup. The two photos show an Au hohlraum filled with  $\sim 0.4$  atm of neopentane gas ( $C_5H_{12}$ ) and containing a CH capsule (30- $\mu$ m-thick, 550- $\mu$ m-diam plastic shell either empty or filled with 50 atm of  $H_2$  gas). A proton backlighter (imploded,  $D^3He$ -filled, thin-glass-shell capsule driven by 30 OMEGA laser beams<sup>15</sup>) is typically 1 cm from the hohlraum center and has the illustrated monoenergetic spectra from the reactions  $D+^3He \rightarrow \alpha + p$  (14.7 MeV) and  $D + D \rightarrow T + p$  (3.0 MeV), recorded with a CR39 detector. The hohlraums had 30- $\mu$ m-thick gold walls, 100% laser entrance hole (LEH), 2.4-mm diameter, and 3.8-mm length. The hohlraum was driven by 30 laser beams with a wavelength of 0.351  $\mu$ m and total laser energy  $\sim 11$  kJ in a 1-ns square pulse. The laser beams had full spatial and temporal smoothing.<sup>16</sup> Radiographic images of (b) proton fluence and (c) proton energy taken with 15-MeV  $D^3He$  protons (the particle energy was slightly upshifted from its birth energy because of the capsule's positive charging) at various implosion times. Within each image, darker means (b) higher proton fluence or (c) lower proton energy. The open arrows in (b) point to the interfaces between the Au wall blowoff and gas plasmas. For the image at 1.65 ns, the solid arrow points to the interface between the capsule ablator and gas plasma.

sule material  $v_{abl} \propto I_{15}^{9/40} \sim C_s$ , the capsule is expected to be essentially unaffected by the pressure generated in this region.<sup>4</sup>

While the proton fluence shows large variations [Fig. 125.7(b)], the proton energy shows less variation [Fig. 125.7(c)] until later times (1.65 ns). This suggests that the trajectories of these backlighting protons have been largely affected by fields around the capsule and not by proton scattering in the plasma because Coulomb interactions are always accompanied by energy loss.<sup>9,14</sup>

To explore the mechanism for forming such a unique spatial (fluence) structure and its effects on impeding the hohlraum wall's plasma expansion and drive dynamics, experiments were performed with solid, spherical CH targets driven in both gas-filled Au hohlraums and CH-lined vacuum Au hohlraums (Fig. 125.9). The two images show related asterisk-like

structures (with spokes in the gaps between pairs of expanding plasma plumes) but with opposite proton fluence distributions: protons were focused into the gaps (high-fluence spokes) for the gas-filled hohlraum [Figs. 125.9(a) and 125.9(c)] but were deflected away from the spokes in the CH-lined vacuum hohlraum [Figs. 125.9(b) and 125.9(d)]. The role of a spontaneously generated magnetic ( $B$ ) field in these interactions can be excluded by symmetry since the toroidal  $B$ -field topology around the laser spots<sup>15,17</sup> cannot result in such azimuthal proton deflections.<sup>9</sup> Lateral electric ( $E$ ) fields<sup>18,19</sup> associated with azimuthally oriented electron pressure gradients ( $\nabla P_e$ ) in the plasma plumes and in the radial plasma jets,  $E = -\nabla P_e / en_e$ , may be the source of these deflections. Another physical mechanism that could explain the deflection near the capsule before 0.5 ns is the  $E$  field associated with a supersonic heat front generated by the laser-heated gas channels that are in close



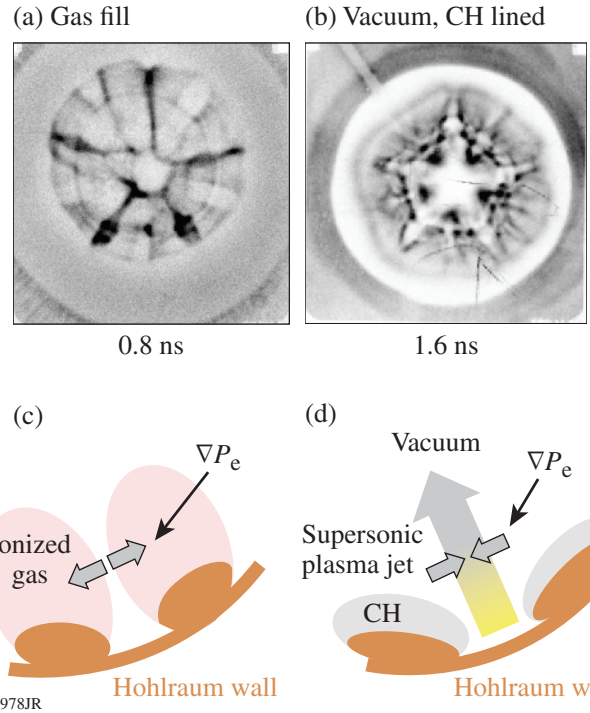
I1977JR

Figure 125.8

Measured interfaces between the Au wall blowoff and the gas plasma (open black diamonds), and between the capsule and the gas plasma (solid red squares), are compared to motion at multiples of the sound speed. The boundary position shown at  $\sim 0.5$  ns suggests that the hot regions of the gas plasma have reached the surface of an imploding capsule at a fast speed ( $\sim 8 C_s$ ). The uncertainties for sampling times were  $\sim 90$  ps (the backlighter burn duration), while for the radius they were  $\sim 10\%$  (the variation in image circularity). The linear fit yields the expansion speed  $v \approx (2.1 \pm 0.3) \times 10^7$  cm s $^{-1}$  (reduced  $\chi^2 = 0.662$ ).

proximity to the capsule. Work is in progress to quantitatively assess the relative importance of this mechanism in the generation of such a field. Since Figs. 125.9(a) and 125.9(b) show opposite deflections,  $E$  must have pointed in opposite directions.

As illustrated in the cartoon in Fig. 125.9(c) for the gas-filled hohlraum, the high plasma pressure should have resulted from an increase of temperature inside the plasma plume and ionized gas.<sup>20</sup> The steep  $\nabla P_e$  results in strong  $E$  fields that point laterally away from the plumes, deflecting the backlighting protons into the gaps between pairs of approaching plasma plumes. For these underdense gas plasmas ( $\sim 0.04 n_{\text{crit}}$ ), the rapidly rising plasma temperature in the region through which the laser passes does not result from continuous laser heating but is a consequence of the inhibition of heat flow caused by the self-generated megaGauss  $B$  field<sup>8,9,11</sup> because the electron thermal transport is reduced by a factor of  $(1 + \omega_{ce}^2 \tau^2)^{-1}$ , where  $\omega_{ce}$  is the electron gyro frequency and  $\tau$  is the collision time.<sup>18</sup> Including the contribution from magnetized window plasma, the Hall parameter  $\omega_{ce} \tau$  is  $\sim 10$  (Ref. 8). Eventually, the combination of inverse bremsstrahlung absorption in the Au wall and electron conduction establishes a near-equilibrium plasma conditions in the laser propagation channel, and the quasi pressure balance leads to continuous plasma heating and temperature increase.<sup>4</sup>



I1978JR

Figure 125.9

The proton fluence distributions show a surplus in the regions between the pairs of expanding plasma plumes in a gas-filled Au hohlraum (a) but show a deficit in a CH-lined, vacuum Au hohlraum (b), indicating opposing directions of the self-generated electric fields as illustrated schematically by the corresponding cartoons, in (c) and (d), respectively.

The spontaneous  $B$  field is generated initially at the hohlraum wall because of nonparallel density and temperature gradients ( $\nabla n_e \times \nabla T_e$ ). Based on the proton deflection feature, the data [Fig. 125.7(b)] show that the plasma temperatures were high<sup>20</sup> even at the earlier time ( $\sim 0.5$  ns) for the fully ionized, low- $Z$  gas plasma whose front boundary had already reached the surface of the imploding capsule within the region of the laser beam's propagation channel, indicating that inhibition of heat flow by fields must have taken place at an earlier time. This suggests that the transport of the field was much faster than the plasma's expansion speed that carried the "frozen in" field with  $[\nabla \times (\mathbf{v} \times \mathbf{B})]$ . The fluid velocity  $v (< C_s)$  is too slow to explain the rapid increase in gas plasma temperature at the earlier times (Figs. 125.7–125.9). Such a nonlocal field transport must have resulted from the convection of the  $B$  field with the heat flux associated with "faster" electrons because of the Nernst effect ( $\propto \beta_\lambda \mathbf{b} \times \nabla T_e$ , i.e., the current flow is driven perpendicular to a  $B$  field and  $\nabla T_e$ , where  $\mathbf{b} \equiv \mathbf{B}B^{-1}$  and  $\beta_\lambda$  is the thermoelectric coefficient perpendicular to the  $B$  field and temperature gradient).<sup>19,21</sup> The velocity of convection of the  $B$  field in this

transport mechanism is approximately  $v_N \approx 2q_e(5n_e T_e)^{-1}$ , where  $q_e = \kappa_{\perp} \nabla T_e$  is the electron heat flux and  $\kappa_{\perp}$  is the thermal conductivity. Using the data from Figs. 125.7(b) and 125.8 (the position of the boundary of the gas plasma that reached the surface of an imploding capsule), a rough estimate indicates that the lower limit for the B-field convection speed is  $v_N \sim 8C_s$ , suggesting that the field transport (convection) by heat flux is about one order of magnitude faster than the plasma expansion ( $v_N \sim 10v$ ). The physical process of the B-field generation, evolution, and dissipation [ $\nabla \times (D_m \nabla \times \mathbf{B})$ ] is described by Faraday's law in a plasma as<sup>18,19</sup>

$$\frac{\partial \mathbf{B}}{\partial t} \approx -\frac{\nabla n_e \times \nabla T_e}{en_e} + \nabla \times (\mathbf{v} \times \mathbf{B}) - \nabla \times (D_m \nabla \times \mathbf{B}) - \frac{\nabla \times \mathbf{R}}{en_e}, \quad (1)$$

where  $D_m$  is the magnetic diffusion coefficient and

$$\mathbf{R} = \frac{(\alpha_{\perp} \mathbf{J}_{\perp} + \alpha_{\parallel} \mathbf{J} \times \mathbf{b})}{en_e} + \beta_{\perp} \nabla_{\perp} T_e - \beta_{\parallel} \mathbf{b} \times \nabla T_e \quad (2)$$

is the contribution of electron thermal and friction forces.<sup>18,19,21</sup> The data suggest that the Nernst effect is responsible for the rapid B-field transport, which is shown to play an important role in observed rapid increase in the gas plasma temperature.

The behavior and dynamics are different in the laser-irradiated, CH-lined, Au vacuum hohlraum [Fig. 125.9(b)]. Although the ablated CH wall helps to compress the Au blowoff, radially moving CH plasma jets are generated with the Au blowoff trailing.<sup>9</sup> This process is initiated by the CH liner ablating from the wall, which subsequently expands with the continual arrival of wall blowoff into the region between the two adjacent expanding plumes. These plasmas collide with one another, leading to the formation of the dense plasma spokes that are redirected radially and move toward the hohlraum interior. The steep  $\nabla P_e$  around the jets results in radial E fields that deflect the imaging protons away from the jets and lead to the asterisk-like spoke structure in the fluence images [Fig. 125.9(d)]. The inward jets travel with supersonic speed ( $\sim 4C_s$ ) generating an early-time stagnation pressure that affects capsule implosion symmetry and dynamics,<sup>9</sup> a phenomenon also observed in the pure vacuum Au hohlraum-driven experiments.<sup>11</sup>

The widths of the spokes in the images can be used with the imaging geometry to estimate the field  $\int \mathbf{E} \times d\ell \sim 3 \times 10^5 \text{ V}$

(where  $d\ell$  is the differential path length along the proton trajectory through the field area).<sup>9</sup> A scale length of  $\sim 0.1 \text{ cm}$  ( $\sim$ laser spot width) for the field in a jet spoke implies  $E \sim 3 \times 10^6 \text{ V cm}^{-1}$ .

To further study the dynamics of the interface and its effect on impeding the plasma stagnation, capsule implosions were performed with a denser hohlraum gas fill ( $\sim 1 \text{ atm}$ ,  $\text{C}_5\text{H}_{12}$ ) at two sampling times (Fig. 125.10). A relatively smooth interface appears between the expanding wall blowoff and the ionized fill gas at 0.8 ns, while chaotic spatial structure and interface interpenetration are evident at 1.6 ns. This interpenetration is caused by hydrodynamic instabilities. The surface perturbations that are seeded at the plume front can be amplified by the classical Rayleigh–Taylor (RT) instability occurring at the interface of the lighter, decelerating ionized gas plasma and the heavier, expanding Au blowoff.<sup>4</sup> This instability has a growth rate<sup>4</sup>  $\gamma_{\text{RT}} \approx (2\pi A_t a k)^{1/2}$ , where  $a$  is the acceleration,  $\sim 10^{16} \text{ cm s}^{-2}$  is estimated from Fig. 125.7(b);  $k = m(2\pi r)^{-1}$  is the perturbation wave number. As an example, for a mode number  $m \sim 50$  at half the hohlraum radius  $r \sim 0.5 \times 0.12 \text{ cm}$ ,  $k \sim 130 \text{ cm}^{-1}$ , and  $A_t = (\rho_2 - \rho_1)/(\rho_2 + \rho_1)$  is the Atwood number at the interface. For  $\sim 0.1 n_{\text{crit}}$  the gas-fill plasma has a  $\rho_1 \approx 3 \text{ mg cm}^{-3}$  while the Au plasma has a  $\rho_2 \approx 10 \text{ mg cm}^{-3}$ ; therefore  $A_t \approx 0.54$ . A rough estimate gives  $\gamma_{\text{RT}} \sim 2.7 \times 10^9 \text{ s}^{-1}$  and a perturbation grows by a factor of  $\sim 15$  in 1 ns. A similar interaction process occurred between the ablated capsule plasma and the gas plasma. The consequence is a reduced benefit of the gas fill because the enhanced interpenetration (or mixing) between the Au blowoff and the gas plasma leads to high-Z material stagnating earlier in the hohlraum interior. This effect does not appear to be

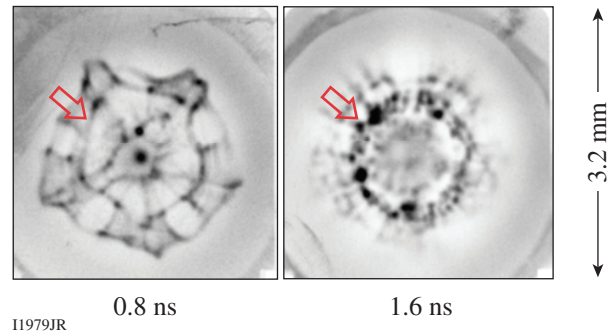


Figure 125.10

Proton fluence images of capsule implosions driven by gas-filled hohlraums. The open arrows point to interfaces between the Au wall blowoff and gas plasma. A relatively smooth interface appears between the expanding wall blowoff and the ionized fill gas at time 0.8 ns, while chaotic spatial structure and interface interpenetration are evident at time 1.6 ns. The fluence surplus inside the imploding capsule (0.8 ns) resulted from self-generated radial E fields.<sup>22,23</sup>

severe because it happens during the coasting phase when the capsule implosion moves at a speed  $v_{\text{imp}}$  that is comparable to, or even faster than, the outward ablation speed ( $\sim C_s$ ). At this time, the high- $Z$  blowoff should be sonically decoupled from the imploding capsule.

To explore the role that CH windows play in impeding the plasma stagnation, we performed capsule implosions driven by vacuum hohlraums with a CH window on both LEH's. This is an important issue because when laser beams pass through the LEH's, the CH windows are immediately evaporated, ionized, and magnetized. The high-pressure, low- $Z$  window plasma will rapidly flow into the hohlraum interior, filling it and altering the wall blowoff dynamics and impeding the plasma stagnation, like the gas fill does. The spontaneous B fields will convect with the flowing window plasma and inhibit electron thermal conduction, further increasing the plasma temperature<sup>18,19,21</sup> and impeding the motion of the wall blowoff. Figure 125.11 shows radiographic images taken while the drive laser was on. Because of the inflow of CH window plasma, no plasma jets formed and the wall blowoff was contained radially. More protons deflected in the radial direction than in the lateral directions of the radial expanding plume. This is because  $|L_T| > |L_n|$ , where  $L_T = T_e(\nabla T_e)^{-1}$  and  $L_n = n_e(\nabla n_e)^{-1}$  are the temperature and density scale lengths, respectively, and  $E \approx |E_r + E_\theta| \propto n_e^{-1} \nabla P_e \sim T_e |L_n^{-1} + L_T^{-1}|$ , leading to  $|E_r| > |E_\theta|$ .

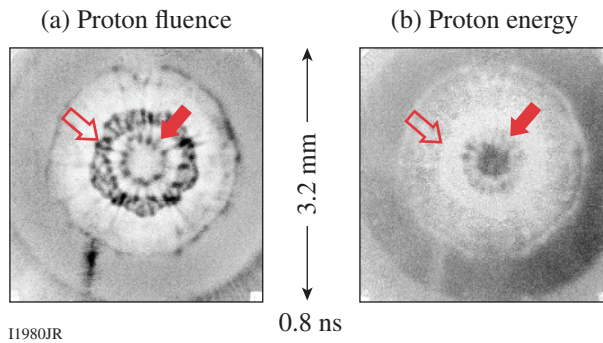


Figure 125.11  
 Images of (a) proton fluence and (b) proton energy from a solid CH sphere driven by a vacuum Au hohlraum with polyimide windows. The open (solid) arrows point to the interfaces between the Au wall blowoff and gas plasma (between the capsule ablation and gas plasma).

In summary, we have performed the first time-gated proton radiography of the spatial structure and temporal evolution of how the fill gas compresses the wall blowoff, inhibits plasma jet formation, and impedes plasma stagnation in the hohlraum interior. We have shown that the plasma interpenetrate

caused by the classical Rayleigh–Taylor instabilities occurs as the lighter, decelerating ionized fill gas pushes against the heavier, expanding gold wall blowoff. We have demonstrated the important roles of spontaneously generated E and B fields in the hohlraum dynamics and capsule implosion. The heat flux is shown to rapidly convect the B field because of the Nernst effect. This experiment provides novel physics insight into the effects of fill gas on x-ray–driven implosions and will have an important impact on the ignition experiments at the NIF.

#### ACKNOWLEDGMENT

This work was supported in part by the U.S. Department of Energy and LLE National Laser User's Facility (DE-FG52-07NA28059 and DE-FG03-03SF22691), LLNL (B543881 and LDRD-08-ER-062), LLE (414090-G), FSC (412761-G), and General Atomics (DE-AC52-06NA 27279). A. B. Zylstra is supported by the Stewardship Science Graduate Fellowship (DE-FC52-08NA28752).

#### REFERENCES

1. J. Nuckolls *et al.*, *Nature* **239**, 139 (1972).
2. R. L. McCrory, J. M. Soures, C. P. Verdon, F. J. Marshall, S. A. Letzring, S. Skupsky, T. J. Kessler, R. L. Kremens, J. P. Knauer, H. Kim, J. Delettrez, R. L. Keck, and D. K. Bradley, *Nature* **335**, 225 (1988).
3. S. W. Haan *et al.*, *Phys. Plasmas* **2**, 2480 (1995).
4. J. D. Lindl, *Inertial Confinement Fusion: The Quest for Ignition and Energy Gain Using Indirect Drive* (Springer-Verlag, New York, 1998).
5. S. Atzeni and J. Meyer-ter-Vehn, *The Physics of Inertial Fusion: Beam Plasma Interaction, Hydrodynamics, Hot Dense Matter*, International Series of Monographs on Physics (Clarendon Press, Oxford, 2004).
6. S. H. Glenzer *et al.*, *Science* **327**, 1228 (2010).
7. O. L. Landen, T. R. Boehly, D. K. Bradley, D. G. Braun, D. A. Callahan, P. M. Celliers, G. W. Collins, E. L. Dewald, L. Divol, S. H. Glenzer, A. Hamza, D. G. Hicks, N. Hoffman, N. Izumi, O. S. Jones, R. K. Kirkwood, G. A. Kyrala, P. Michel, J. Milovich, D. H. Munro, A. Nikroo, R. E. Olson, H. F. Robey, B. K. Spears, C. A. Thomas, S. V. Weber, D. C. Wilson, M. M. Marinak, L. J. Suter, B. A. Hammel, D. D. Meyerhofer, J. Atherton, J. Edwards, S. W. Haan, J. D. Lindl, B. J. MacGowan, and E. I. Moses, *Phys. Plasmas* **17**, 056301 (2010).
8. S. H. Glenzer *et al.*, *Phys. Plasmas* **6**, 2117 (1999).
9. C. K. Li, F. H. Séguin, J. A. Frenje, M. Rosenberg, R. D. Petrasso, P. A. Amendt, J. A. Koch, O. L. Landen, H. S. Park, H. F. Robey, R. P. J. Town, A. Casner, F. Philippe, R. Betti, J. P. Knauer, D. D. Meyerhofer, C. A. Back, J. D. Kilkenny, and A. Nikroo, *Science* **327**, 1231 (2010).
10. J. M. Soures, R. L. McCrory, C. P. Verdon, A. Babushkin, R. E. Bahr, T. R. Boehly, R. Boni, D. K. Bradley, D. L. Brown, R. S. Craxton, J. A. Delettrez, W. R. Donaldson, R. Epstein, P. A. Jaanimagi, S. D. Jacobs, K. Kearney, R. L. Keck, J. H. Kelly, T. J. Kessler, R. L. Kremens, J. P. Knauer, S. A. Kumpan, S. A. Letzring, D. J. Lonobile, S. J. Loucks,

- L. D. Lund, F. J. Marshall, P. W. McKenty, D. D. Meyerhofer, S. F. B. Morse, A. Okishev, S. Papernov, G. Pien, W. Seka, R. Short, M. J. Shoup III, M. Skeldon, S. Skupsky, A. W. Schmid, D. J. Smith, S. Swales, M. Wittman, and B. Yaakobi, *Phys. Plasmas* **3**, 2108 (1996).
11. C. K. Li, F. H. Séguin, J. A. Frenje, R. D. Petrasso, P. A. Amendt, R. P. J. Town, O. L. Landen, J. R. Rygg, R. Betti, J. P. Knauer, D. D. Meyerhofer, J. M. Soures, C. A. Back, J. D. Kilkenny, and A. Nikroo, *Phys. Rev. Lett.* **102**, 205001 (2009).
  12. R. P. Drake, *High-Energy-Density Physics: Fundamentals, Inertial Fusion, and Experimental Astrophysics*, Shock Wave and High Pressure Phenomena (Springer, Berlin, 2006).
  13. For an adiabatic rarefaction expansion of an ideal gas, the expansion speed is  $3 C_s$  in vacuum, while the hot electrons advancing ahead of the rarefaction expansion because of their high mobility may further boost the motion of leading edge CH and Au ions ablating off the hohlraum wall by an additional  $C_s$  factor.<sup>9</sup>
  14. C. K. Li and R. D. Petrasso, *Phys. Rev. Lett.* **70**, 3059 (1993).
  15. C. K. Li, F. H. Séguin, J. A. Frenje, J. R. Rygg, R. D. Petrasso, R. P. J. Town, P. A. Amendt, S. P. Hatchett, O. L. Landen, A. J. MacKinnon, P. K. Patel, V. A. Smalyuk, T. C. Sangster, and J. P. Knauer, *Phys. Rev. Lett.* **97**, 135003 (2006).
  16. D. D. Meyerhofer, J. A. Delettrez, R. Epstein, V. Yu. Glebov, V. N. Goncharov, R. L. Keck, R. L. McCrory, P. W. McKenty, F. J. Marshall, P. B. Radha, S. P. Regan, S. Roberts, W. Seka, S. Skupsky, V. A. Smalyuk, C. Sorce, C. Stoeckl, J. M. Soures, R. P. J. Town, B. Yaakobi, J. D. Zuegel, J. Frenje, C. K. Li, R. D. Petrasso, D. G. Hicks, F. H. Séguin, K. Fletcher, S. Padalino, C. Freeman, N. Izumi, R. Lerche, T. W. Phillips, and T. C. Sangster, *Phys. Plasmas* **8**, 2251 (2001).
  17. R. D. Petrasso, C. K. Li, F. H. Séguin, J. R. Rygg, J. A. Frenje, R. Betti, J. P. Knauer, D. D. Meyerhofer, P. A. Amendt, D. H. Froula, O. L. Landen, P. K. Patel, J. S. Ross, and R. P. J. Town, *Phys. Rev. Lett.* **103**, 085001 (2009).
  18. S. I. Braginskii, in *Reviews of Plasma Physics*, edited by Acad. M. A. Leontovich (Consultants Bureau, New York, 1965), Vol. 1.
  19. M. G. Haines, *Phys. Rev. Lett.* **78**, 254 (1997).
  20. Such a temperature rise has been seen with Thomson scattering in Nova experiments, where an electron temperature  $\sim 2$  keV was measured on the axis of a gas-filled hohlraum at early times during a 1-ns laser pulse ( $I \approx 10^{15}$  W/cm<sup>2</sup>), and in LASNEX simulations of the development of hot regions along the laser-pass channel.<sup>8</sup>
  21. A. Nishiguchi *et al.*, *Phys. Rev. Lett.* **53**, 262 (1984).
  22. C. K. Li, F. H. Séguin, J. R. Rygg, J. A. Frenje, M. Manuel, R. D. Petrasso, R. Betti, J. Delettrez, J. P. Knauer, F. Marshall, D. D. Meyerhofer, D. Shvarts, V. A. Smalyuk, C. Stoeckl, O. L. Landen, R. P. J. Town, C. A. Back, and J. D. Kilkenny, *Phys. Rev. Lett.* **100**, 225001 (2008).
  23. P. A. Amendt *et al.*, *Plasma Phys. Control. Fusion* **51**, 124048 (2009).